The Meteoritical Society

*Meteoritics & Planetary Science* 42, Nr 4/5, 755–768 (2007)
Abstract available online at http://meteoritics.org

# In situ seismic measurements in borehole LB-08A in the Bosumtwi impact structure, Ghana: Preliminary interpretation

D. R. SCHMITT[1*], B. MILKEREIT[2], T. KARP[3, 4], C. SCHOLZ[3], S. DANUOR[5], D. MEILLIEUX[1], and M. WELZ[1]

[1]Institute for Geophysical Research, Department of Physics, University of Alberta, Edmonton, Alberta, T6G 2G7, Canada
[2]Department of Physics, University of Toronto, 60 Saint George Street, Toronto, Ontario, M5S 1A7, Canada
[3]Department of Geology, 204 Heroy Geology Laboratory, Syracuse University, Syracuse, New York 13244, USA
[4]Geophysik GGD, Ehrensteinstrasse 33, 04105 Leipzig, Germany
[5]Department of Physics, Kwame Nkrumah University of Science and Technology, Kumasi, Ghana
[*]Corresponding author. E-mail: doug@phys.ualberta.ca

*(Received 01 October 2006; revision accepted 10 February 2007)*

**Abstract**–In order to assist in the interpretation of previous seismic refraction and reflection surveys, a vertical seismic profile was acquired in the Lake Bosumtwi (Ghana) hard-rock core hole LB-08A. No seismic reflections are seen in the up-going wave field obtained, and this observation is consistent with the lack of reflectivity observed in the corresponding 2-D surface seismic profile obtained in earlier studies. Direct down-going P-waves were found both in the cased sediment column from a depth of 73 m to 239 m below the lake surface and in the open-hole "hard rock" section from a depth of 239 m to 451 m of LB-08A. Analysis of the observed travel times indicates a nearly constant P-wave velocity of 1520 m/s through the soft lacustrine sediments. In the hard-rock, however, the P-wave velocity rapidly increases by nearly 30% from 2600 m/s to 3340 m/s. These values are in good agreement with the gross velocity structure obtained in the earlier joint inversion of seismic reflection and refraction data. These values are low relative to those expected for the metasedimentary protoliths, an observation that has been made at other young impact structures of similar size. The low velocities, together with the fact that they increase so rapidly, is suggestive of a decreasing density of fractures and microcracks with depth. Consequently, the seismic velocity trend may provide a proxy measure of damage, and hence, the decay of the shock pressure from the impact point. Validation of this requires additional detailed studies of the porosity structure in the core.

## INTRODUCTION

The Bosumtwi impact crater is a 1.07 Myr old impact structure thought to be the source of the Ivory Coast tektites (Koeberl et al. 1997). The impact structure is approximately 10.5 km in rim-to-rim diameter but the base of the crater is concealed by Lake Bosumtwi, which is 8 km in diameter (Fig. 1).

Field geological investigations of the crater structure are restricted by both Lake Bosumtwi and the thick layer of soft sediments that have accumulated in it since the crater's formation. Consequently, geophysical magnetic, gravity, and seismic methods must play a major role in delineating the structure of the crater. Marine reflection seismic investigations (Fig. 2), in particular, revealed the existence of a prominent central uplift surrounded by a circular depression (Scholz et al. 2002).

The current study was carried out as part of the interdisciplinary Lake Bosumtwi Drilling Project of the International Continental Scientific Drilling Program (ICDP) of 2004. The work here focuses on recording the seismic wave field at depth in order to learn more about the in situ seismic properties of the sediments and the impacted rocks along the extent of the borehole. To our knowledge, this may be the first attempt anywhere to obtain in situ information about the detailed seismic velocity structure within such a young impact structure; and as such this complements other surface reflection and refraction studies at Bosumtwi (Karp et al. 2002) that have been used to provide areally extensive but low resolution mapping of the impact in terms of its remaining seismic velocity structure. An initial analysis of the seismic data here suggests that the seismic velocities observed in the hard-rock portion of the drilling are substantially reduced relative to those anticipated for such crystalline metamorphic lithologies.

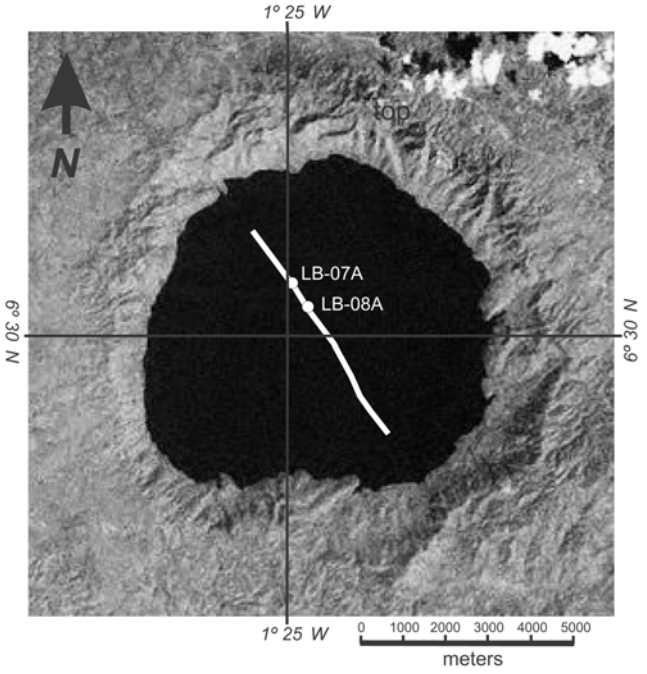


Fig. 1 Aster satellite image of Lake Bosumtwi with the positions of the boreholes LB-07A and LB-08A sited along the seismic profiles of Figs. 2 and 3.

## BACKGROUND

Prior to describing the field measurements, it is worthwhile to briefly review previous seismological studies over meteorite impact sites. Many of these studies show that the impacted material is characterized by strikingly low velocities relative to the same undamaged rock. The damaged rock has a high density of fractures and microcracks; a brief review of the effects of such damage on the wave speeds in rock is given. Further, the vertical seismic profiling techniques employed are briefly described, as the methods are specialized and, to our knowledge, have not previously been employed to study directly an impact structure.

### Local Geology

The geology of the area has recently been reviewed by Koeberl and Reimold (2005) who provided a comprehensive history of geological studies in and around Lake Bosumtwi. The impact structure lies in the ~2 Gyr old metasediments and metavolcanics of the Birimian Supergroup (Jones et al. 1981). The rock types intersected by the ICDP cores consist primarily of meta-graywacke, phyllites, and shales that have been subject to lower greenschist metamorphic conditions (Coney et al. 2007; Deutsch et al. 2007; Ferrière et al. 2007). In addition, a small granitoid component was part of the target volume (Reimold et al. 1998; Coney et al. 2007). A unique seismic velocity cannot be ascribed to a rock type on the basis of its geological description. However, the compressional wave velocities of such rocks in a pore-free undamaged state would generally exceed 5500 m/s (e.g., Christensen and Mooney 1995; Ji et al. 2002).

### Seismological Investigations of Impact Structures

There are two primary types of seismic investigations carried out from the surface: reflection or refraction (e.g., Lay and Wallace 1995). Surface seismic reflection imaging, whether it is 2-D or 3-D, provides high resolution indications of the seismic wave transit times to discontinuities in the lithologically dependent elastic physical properties and as such gives detail of geological structure (e.g., Yilmaz 2001). Reflection profiling does not, however, provide accurate measures of in situ seismic velocities. Conversely, refraction seismic methods provide relatively good measures of the in situ seismic wave speeds but at a cost of poor vertical and lateral resolution. Borehole seismology, the method employed in this study, is able to provide better measures of in situ material velocities and to exactly tie travel time to a given depth in the earth—but at the cost of more limited area coverage.

Pilkington and Grieve (1992) provided an overview of reflection and refraction studies, and Harris et al. (1991) listed a number of impact structures that had been imaged by reflection profiling over impact structures up to the early 1990s. The structures as delineated by seismic means depend on many variables such as the volume and extent of melt sheets, the amount of brecciation or damage, and the size of the structure. The number of seismological studies of impact structures has grown substantially over the last few years with studies at scales ranging from hundreds of kilometers over large impact structures such as Chicxulub in Mexico (Morgan et al. 2000) and Sudbury (Wu et al. 1995; Boerner et al. 2000) to smaller structures such as the Mjølnir structure in the Barent Sea, which is ~40 km in diameter (Dypvik et al. 2004) and the buried (but not yet confirmed to be an impact) Silverpit structure, which is ~10 km in diameter, that was well resolved in 3-D seismic images (Stewart and Allen 2005). The age range for these seismically studied structures extends from the 2.02 Gyr old Vredefort-Witwatersrand structure of South Africa (cf. Gibson and Reimold 2001, 2005) to the 49.7 kyr old Barringer impact structure (e.g., Phillips et al. 1991).

Differences in sizes and ages make comparison of the known impact structures problematic. For example, the Proterozoic (~1850 Myr) Sudbury structure has experienced substantial tectonic metamorphism and deformation since its creation. These processes have long since erased the signature of the impact upon the rock's elastic physical properties. Other factors including the existence of thick melt sheets such as the Sudbury Igneous complex (Therriault et al. 2002) or of the central uplift of deeper and higher velocity materials as

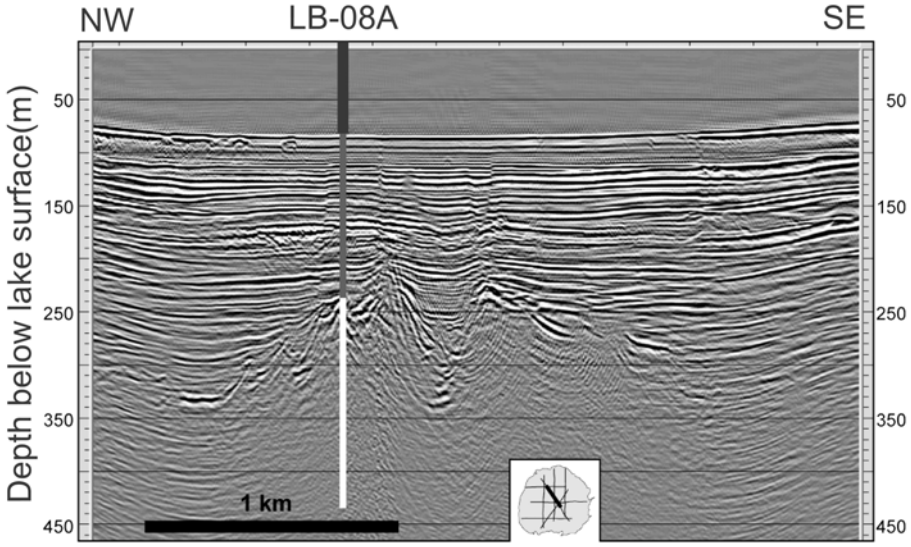


Fig. 2. A depth-converted reflection seismic profile over the center of Lake Bosumtwi showing the central peak and the location of borehole LB-08A (UTM Zone 30, 675553.49 m E, 719755.58 m N). Black vertical line: 73 m deep water column contained with riser; gray line: temporary PQ dimension steel casing through riser and lacustrine sediments to 239 m depth; white line: HQ dimension open hole in through hard rock impactites and shock damaged protolith rock to 451.3 m depth. Figure is adapted from Scholz et al. (2002).

seen at Chicxulub (Morgan et al. 2000) and Vredefort (Green and Chetty 1990; Durrheim and Green 1992) further complicates comparison of the larger structures to those at the scale of the Bosumtwi impact structure.

Studies for which a comparison is more germane to the present work include the Quaternary (49.7 kyr) Barringer crater, Arizona (Ackermann et al. 1975), the early Cretaceous (~121 Myr) Lake Mien (Åström 1998), and the Devonian (~360 Myr) Siljan (Papasikas and Julian, 1997) structures in Sweden, the Pliocene (~3.6 Myr) El'gygytgyn crater, Siberia (Gebhardt et al. 2006), the Miocene (~15 Myr) Ries crater, Germany (Wünnemann et al. 2005), the Miocene (~22 Myr) Haughton crater, Canada (Hajnal et al. 1988; Scott and Hajnal 1988), the Pleistocene (~0.8 Myr) Zhamanshin crater, Siberia (Florensky and Dabizha 1980; Karp et al. 2002), and of course the Pleistocene (~1.07 Myr) Bosumtwi impact structure itself. Similar effects are seen in the vicinity of craters created by large man-made explosions (Ackermann et al. 1986). The diameters of these comparable craters range from less than 1 km to more than 20 km; they do not fall into the same category when considered from the point of view of their geological complexity. However, they do all share the same characteristic of a pronounced lowering of seismic wave speeds relative to those for the pre-impact protolith. In the vicinity of and beneath impact structures the seismic velocities are lower, sometimes quite substantially, than those of the original protolith.

One of the earliest crater scale seismological studies was that of Ackermann et al. (1975) who carried out what may be one of the first directed seismological studies at Barringer crater, Arizona (~1200 m in diameter), not all that long after it was confirmed and accepted that it was produced in an impact event. Ackermann et al. (1975) conducted a series of kilometer-scale refraction tests that transected the crater, and they showed that the seismic velocity both beneath and laterally adjacent to the crater was considerably lower than measured for the same geological formations at least 900 m removed from the crater. Specifically, they detected a roughly conically shaped zone of low velocity, which they inferred to be breccia and fractured country rock extending as far as 900 m out from the rim crest and as deep as 800 m beneath the crater floor. On the basis of the travel time delays in the vicinity of the crater they suggested that the seismic P-wave velocity of the Coconino sandstone had been reduced by ~30% from ~3000 m/s to ~2250 m/s.

Similarly, the interpretation of latest refraction work at El'gygytgyn suggests an upper and a lower "brecciated" zone with velocities of ~ 3 km/s and > 3.6 km/s, both of which are lower than the ~ 5 km/s velocities of the nearby undisturbed crystalline rocks (Gebhardt et al. 2006). At the Ries structure, too, recent re-analysis (Wünnemann et al. 2005) of seismic refraction profiles collected in the 1970s (Pohl and Will 1974; Pohl et al. 1977) showed velocities as low as 2 km/s within the crater, which contrast with the 6 km/s velocity of the surrounding granitic protolith.

Unfortunately, there are fewer reports of S-wave velocities near such structures. The earlier work on the older and highly eroded Lake Mien structure includes estimates of both P- and S-wave velocities based on inversion of body wave arrival times and surface wave dispersion curves. Except for the zone immediately at the center of impact, both the P- and S-wave velocities are diminished in the vicinity and beneath the largely eroded crater (Åström 1998).

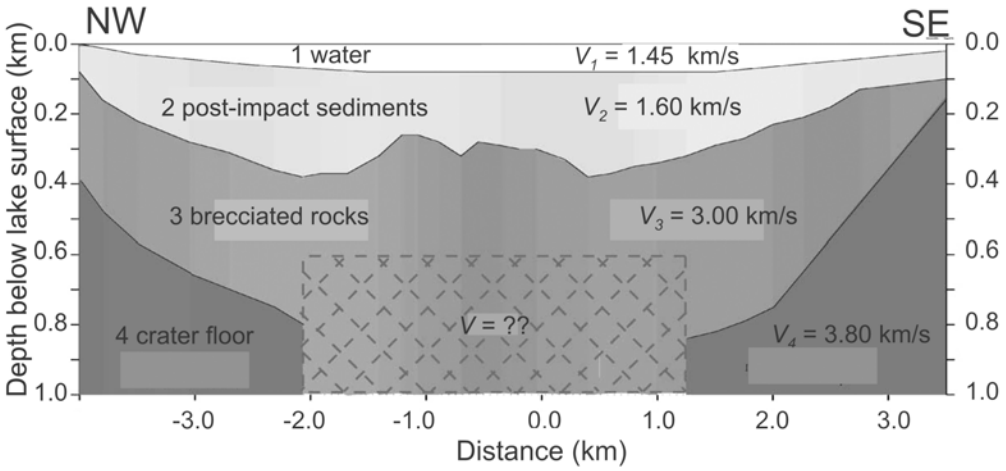


Fig. 3. Interpreted NE-SW seismic velocity transect as determined by joint analysis of both reflection and refraction records across Lake Bosumtwi. Image reprinted from Karp et al. (2002) with permission from Elsevier.

Previously at Bosumtwi, Karp et al. (2002) analyzed both refraction and reflection data acquired in a series of marine surveys over the lake. They interpreted these data with a final 4 layer model of lake water (1.45 km/s), post-impact lacustrine sediments (~1.6 km/s), so-called "brecciated" rocks (3.0 km/s) and crater floor rocks (3.8 km/s), as illustrated in Fig. 3. Unfortunately, there is no information at this time on the seismic velocities outside of the deformation zone, but as noted above, given the metamorphic crystalline nature of the target rock, one must expect that the P-wave velocity of the intact rock is greater than 5.5 km/s.

**Shock Damage and Seismic Wave Velocity**

Chemical composition aside, the most important factor that influences the elastic properties and hence the seismic wave speeds of a given lithology is the porosity; the greater the porosity, the lower the wavespeed. This last statement unfortunately oversimplifies the relationship between porosity and velocity, and many other elements, particularly the type of porosity encountered, can have a large effect (e.g., Knight and Nolen-Hoeksema 1990). In a first simplification, one may consider the pore space of a rock to consist of either equant "spherical" pores or low aspect-ratio, crack-like planar pores. The latter are compliant and will progressively close as confining stress is applied. Even a small amount of such crack-like porosity will strongly influence the elastic properties of materials in general.

The effect of such microcracks has long been recognized, ever since the first measurements of wave speeds on crustal rocks had been performed by Adams and Williamson (1923). A variety of workers have further demonstrated this experimentally or have developed theoretical descriptions to describe the reduction in strength, elastic moduli, and wave speeds (e.g., O'Connell and Budiansky 1974) but a review of this is beyond the scope of this article.

A number of experimental studies (e.g., Polanskey and Ahrens 1990; Ahrens and Rubin 1993; He and Ahrens 1994; Liu and Ahrens 1997; Xia and Ahrens 2001; Ai and Ahrens 2004, 2007, to name only a few) have shown that impact processes induce microcrack damage in rock and that the density of microcracks and the subsequent decline in P- and S-wave velocities depend on the severity of the impact deformation Consequently, the decline of seismic velocities beneath impact craters and the sites of large explosions is due to the production of crack-like porosity which may occur at many scales and can be produced by a variety of the processes from the initial shockwave itself to deformation during rebound. Indeed, the velocity deficit produced by the impact has some potential to be a proxy measure of the local shock pressure encountered by the material. This is emphasized in the recent work of Collins et al. (2004) who incorporated strain-dependent damage into their modeling of the development of an impact structure ~10 km in diameter. This damage leads to a lowering of both mass density and seismic velocities.

**Vertical Seismic Profiling**

Vertical seismic profiles (VSP) typically consist of recording, at a uniformly spaced set of depths within the earth, the seismic waves produced by a surface energy source. Texts by Hinds et al. (1996) and Hardage (2000) provide good overviews of this technique. Essentially, a series of seismic waveforms is obtained by lowering seismic receivers to set depths in a well-bore using a wire-line. The observed waveforms are recorded as functions of time and then plotted against depth to produce the profile. The profiles reveal a great deal about the transit times of various seismic waves to a given depth in the earth, on the character of the down-going seismic pulse, on the locations of different seismic reflectors seen in complementary reflection surface profiles, and on in situ properties such as wave speed and attenuation.

It is useful to first provide a brief description of what is to be expected in a borehole VSP measurement, as many workers are not familiar with this technique. As noted above, seismic traces are acquired at a series of depths in the earth. The style of recording here is often referred to as a "zero-offset" VSP, which indicates that the source is placed at a single point at the surface close to the borehole; the seismic raypaths from the source to the receiver are consequently nearly vertical and have lengths that are very close to the depth of the receiver. Figure 4a shows a cartoon of this geometry in a simplified geology consisting of two layers of different seismic velocities together with the locus of the travel time curves for the directly arriving waves. The velocity of a given wave in a depth interval along the borehole influences the slope of the depth-time arrival curve; and, for example, the lower velocities in layer 1 manifest themselves as a z-t curve with lower dip than in layer 2 (Fig. 4b). Note that the slope of the up-going reflected wave dips in the opposite direction but with the same absolute value of velocity (Fig. 4d).

VSP data are also often used to find the depths at which seismic reflections originate and hence assist in the interpretation of surface reflection seismic profiles. With real VSP data this is problematic because even for the strongest reflections the amplitude of the down-going wave pulse from the source exceeds that of the up-going reflection by factors of 10 or more. As such, the down-going wave field masks the up-going wave field sufficiently, so that the latter cannot be interpreted or often even reliably detected by visual analysis of a raw profile. To overcome this problem, a variety of image processing techniques are applied to the 2-D profile to separate the down-going pulse from the camouflaged up-going reflections (Seeman and Horowicz 1983; Kommendal and Tjostheim 1989). This is simply illustrated in Fig. 4, which shows the idealized down-going (Fig. 4c) and up-going (Fig. 4d) arrivals after separation from the complete observed seismic arrivals of Fig. 4b. Some of the more popular separation methods include 2-D Fourier transform (f-k) filtering (Yilmaz 2001), the related τ-p slant-stack technique (Moon et al. 1986), and the median filtering method (Hinds et al. 1996). Median and f-k filtering are applied here, some more detail about this is provided in the next section.

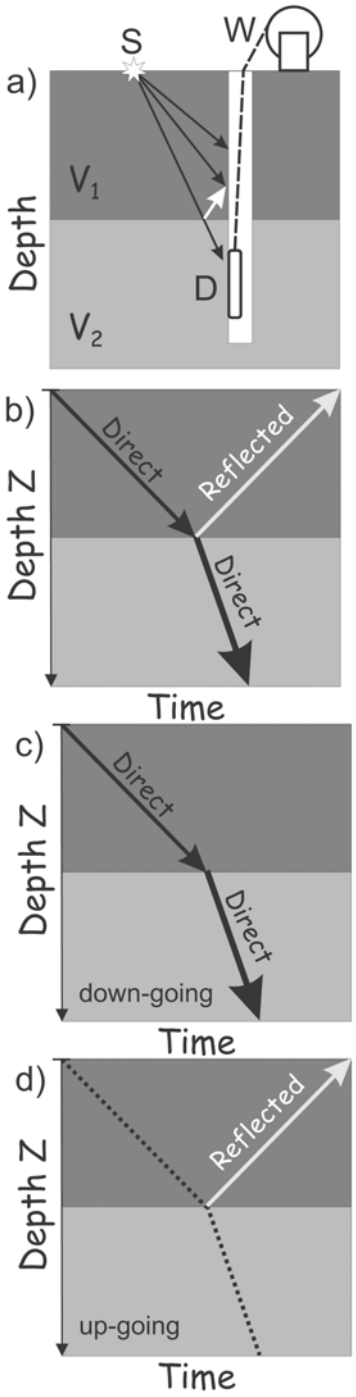


Fig. 4. A simple illustration of the geometry of a vertical seismic profile experiment. a) Field geometry with seismic source S producing seismic wave field that propagates along ray paths to a sequence of depths to receiver D. The receiver is moved to a sequence of set depths by wire-line and winch W. The simplified geological structure consists of top and bottom layers with seismic velocities V1 and V2 > V1. b) Resulting travel time curves for the direct wave through both layers and for a seismic reflection produced at the geological interface between the layers. c) and d) illustrate the down-going and up-going wave fields, respectively, obtained from the observed data after wave field separation.

## SEISMIC DATA ACQUISITION

Conventional VSPs are typically obtained at relatively large receiver spacings of 10 m or more, primarily because of economic cost and the time required to acquire such data sets. Here, a similar approach but with a much more frequent spatial depth sampling at a 1 m spacing was taken to obtain information on the in situ seismic velocities in the second hard-rock borehole LB-08A at Lake Bosumtwi.

The VSP acquisition operation was carried out from the DOSECC GLAD-800 floating platform (Fig. 5) positioned

Fig. 5. A photograph of the GLAD-800 at Lake Bosumtwi.

near the center of the impact structure. At completion of drilling the configuration of LB-08A (Fig. 6) consisted of i) a 73 m high steel riser (ID = 223 mm) beneath the GLAD-800 to the lake bottom to allow for drilling with fluid circulation, ii) a temporary and uncemented PQ-dimension (nominal bit diameter = 122.6 mm) steel casing (inside diameter = 114.3 mm) consisting of the drill rod from the drill floor through the water column and weakly consolidated lake sediments to the top of the indurated impactites at 239 m, with iii) HQ-dimension (nominal bit diameter = 95.6 mm) open hole beneath this to a depth of 451.3 m. This geometry is important because, as will be seen, it strongly influenced the observed seismic records in the cased section.

During operations, the support boat RV Kilindi operated by Syracuse University was tied to the side of the DOSECC managed GLAD-800 barge. A single air gun (0.65 l displacement) was lowered from her side into the lake water to a water depth of 3 m and with an approximately 14 m offset from the top of the borehole. The air gun provided a seismic pulse by the rapid opening of a valve that releases compressed air at pressures in excess of 15 MPa into the water. The air gun was manually fired from the compressor system on the Kalindi. A piezoelectric element immediately on the air gun was directly connected to the trigger sensing electronics of the data acquisition system; and the electronic pulse produced by this element triggered data recording.

The receiver consisted of a wire-line wall-locking 3-component geophone tool (Manufactured by SIE Pty, Australia). This tool carries two horizontal geophones and one vertical 14 Hz geophone in an orthogonal geometry. The output of these geophones is amplified downhole in order to accommodate the long transmission through the wireline. The semi-portable logging system provided by the GeoForschungsZentrum (Potsdam) logging team carried sufficient conductors to allow only the response of the vertical component geophone to be recorded. The seismic records, obtained at 1 m intervals along the borehole from 451 m to 50 m below the lake surface were sampled at 125 μs with a pre-trigger time of 220 ms and a listening time of 1828 ms. Acquisition was accomplished using a Geode system (Geometrics Group Inc., California). The data were obtained over a period of approximately 15 daylight hours on October 1 and 2, 2004.

## SEISMIC DATA PROCESSING AND RESULTS

The primary motivations of the VSP survey were to further examine the nonreflecting or “transparent” character of the seismic reflection profile (Fig. 2) within the hard rock below the impact crater and to obtain detailed information on the seismic velocities within those parts of the structure accessible to drilling.

With regards to the latter, the material velocities were estimated from the directly measured travel times for the various seismic arrivals as discussed in the next section. The first arriving compressional wave is apparent in all the records to the greatest depth encountered, and as such minimal processing was required for this purpose. Only cosmetic processing was carried out and included quality control checking and trace energy equalization in order to improve visualization of the lower and weaker traces relative to those nearer the source (Fig. 6). This record is quite complex, particularly in the PQ cased section of the well bore above the hard rock top at 239 m; and a number of features require attention.

For a given arrival, the times of the first coherent amplitude peak of each waveform were picked manually. We avoided the more popular “first break” time picking method, which usually consists of selecting the first point at which the arrival is recognized, because of i) greater uncertainty and more opportunity for subjectivity particularly for later arrivals that are partially obscured by earlier arrivals, ii) the importance of relative times between depths in opposition to absolute arrival times at depth to allow for more accurate estimations of interval velocities, and iii) the theoretical ambiguity of the meaning of a velocity derived from the “first break” time of a pulse propagating in an attenuating medium (Molyneux and Schmitt 2000).

The travel times of the four different down-going arrivals of the extensional casing wave, the direct compressional wave in the lake sediments and continuing into the hard rock, and a possible shear or secondary wave are plotted in Fig. 7. Derivation of the in situ wave speeds from these results follows in the next sections.

It is necessary to examine the signal character, which is influenced by a number of factors. First, the bubble produced in the water column by the air gun reverberates as it rises to the surface; this oscillation considerably lengthens the effective input seismic wavelet (e.g., Johnson 1994). This oscillation has a period of ~50 ms as seen in Fig. 6 and is

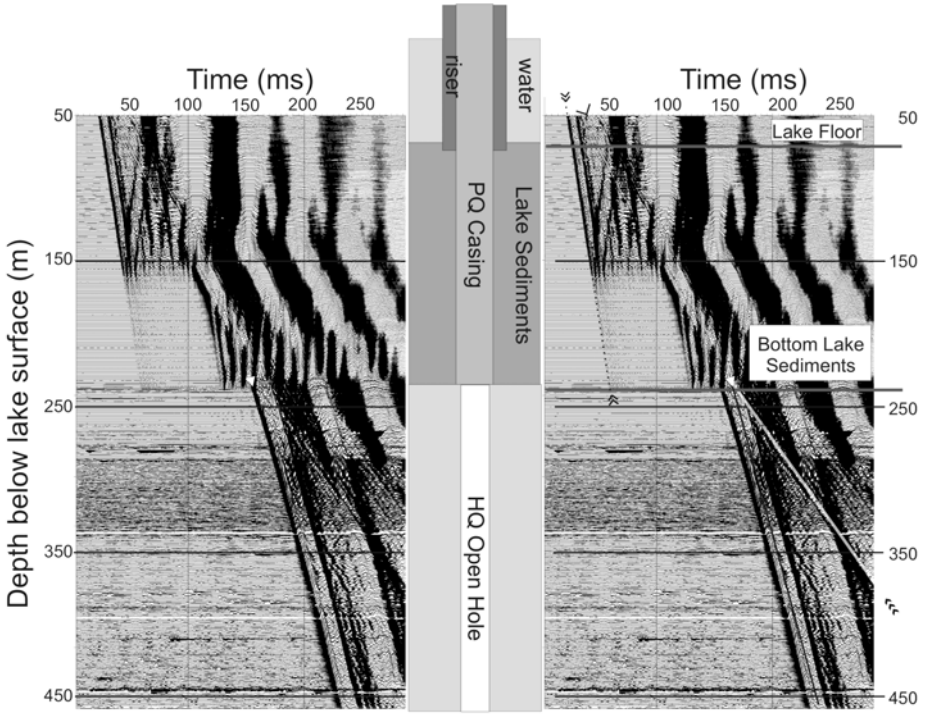


Fig. 6. Left: Unprocessed vertical seismic profile of recorded vertical geophone response. Right: same profile record but with interpretations of various arrivals indicated by arrows (arrival through steel PQ casing (0 m to 239 m, thin double arrow heads between dotted line), direct P-wave arrival through water and lacustrine sediments (0 to 239 m, thin single arrowhead at top only), direct P-wave arrival through hard rock (between white thick arrowhead and black thick arrowhead) and weak secondary converted arrival through hard rock. Center: borehole geometry from lake surface ($z$ = 0 m) to bottom of open holes section (depth = 451.3 m).

particularly evident in the profile at depths near 165 m. This low frequency (~20 Hz) of this reverberation allows it to be removed by Fourier bandpass filtering, as can be seen in the comparison of Fig. 8a and Fig. 8b. Second, the waveform is complicated initially by the ghost of the initial pulse reflected from the lake surface (only 4 ms later) and by water column reverberations (with a period of ~100 ms). This can be a serious issue in seismic reflection profiling, as the reverberating bubble pulse and the multiples denigrate the vertical resolution of the image. A variety of deconvolution processing strategies are employed to attempt to overcome these problems (Hargreaves 1992; Amundsen et al. 2001). However, deconvolution as normally practiced is imperfect (Ziolkowski 1991), and while it may be necessary for conventional 2-D or 3-D seismic imaging, it was not needed in this VSP study.

As noted, two different wave field separation methods were employed. These were applied only for the open-hole hard rock section of the profiles because the lack of seismic reflectivity in this section was of scientific interest. Furthermore, as will be seen below, the profile through the cased section is contaminated with numerous additional borehole modes. The technical application of these techniques is beyond the needs of this contribution; extensive descriptions may be found in the references cited. They were applied using a combination of commercial (Vista seismic

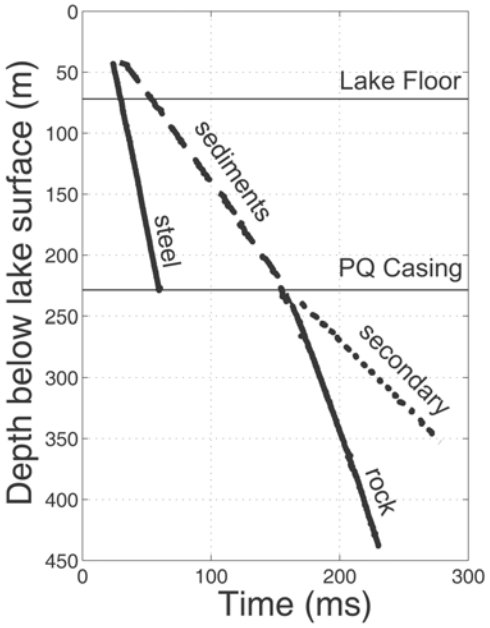


Fig. 7. Observed travel times of the extensional wave through the PQ steel casing, the compressional waves through the lake water and sediments (sediments) and through the open hole section of the well bore (rock), and the undefined secondary wave through the open hole. The size of the symbols employed exceeds the relative uncertainties of both depth (~10 cm) and travel-time (~0.5 ms).

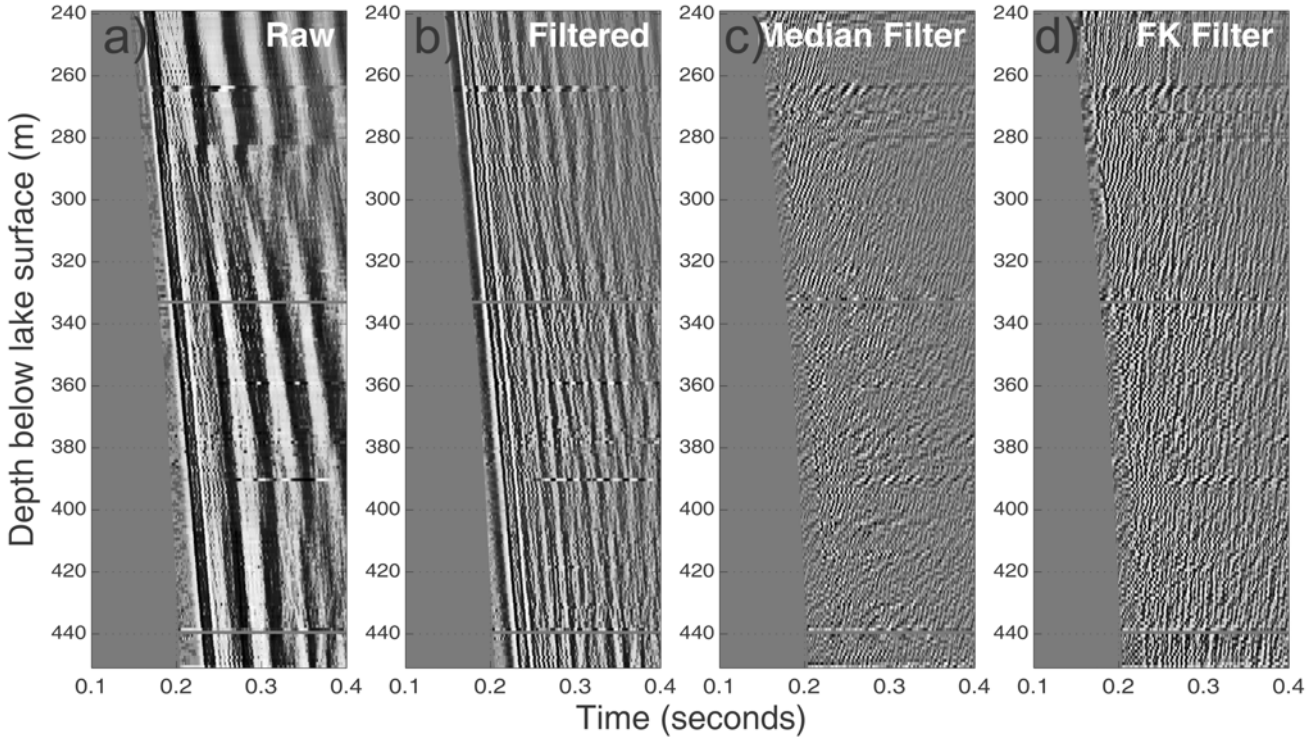


Fig. 8. The results of wave field separation through hard rock section of well bore. a) An expanded view of raw seismic profile extracted from Fig. 6 over the window from a depth of 239 m to 451 m and 0.1 s to 0.4 s time. b) After application of a 1-D temporal bandpass filter (Ormsby window with corners at frequencies of 40 Hz-50 Hz-250 Hz-400 Hz). c) Up-going wave field as obtained from (a) using 2-D median filtering. d) Up-going wave field as obtained using 2-D f-k filtering.

processing software provided by Seismic Image Software Inc.) and written codes (Matlab by the Mathworks Inc.). However, simplified processing flows for obtaining the up-going wave fields are presented in Tables 1 and 2 for the median and the f-k methods, respectively, with the final results presented in Fig. 8.

## DISCUSSION

### Interpretation of Separated Wave Fields

Karp et al. (2002) and Scholz et al. (2002, 2007) noted the lack of seismic reflections within the hard rock zone beneath the lake sediments in their seismic reflection profile (compare Fig. 2). The up-going wave fields of Figs. 8c and 8d, calculated using two different methods, support this observation; there are no apparent up-going reflections in these images.

L'Heureux and Milkereit (2007) point out that similar behavior has been seen in reflection profiles over other large impact structures. They suggest that the lack of reflectivity is due to impact induced heterogeneity, i.e., the scale of the mixing of the materials within the damaged zone is smaller than the resolution limit of seismic analysis.

Tube waves are one additional characteristic of these records that are worthy of note primarily because they are absent in both the full (Fig. 6) and the up-going (Fig. 8) wavefields in the open-hole. This is somewhat unexpected as tube waves are usually produced where fractures intersect the borehole (e.g., Beydoun et al. 1985) and are a serious obstacle in interpretive processing. The theory of their production is sufficiently developed that their analysis can provide constraints on both the geometry and hydraulic transmissivity of the fractures (Cicerone and Toksöz 1995), although a fracture from which a tube wave originates does not necessarily need to be permeable (Li et al. 1994). The formation along the open hole is expected to be highly fractured; the absence of detectable tube waves is thus unexpected.

### Cased Hole Section

The first arrival seen in the PQ cased section of the well bore is highlighted in the interpreted right panel of Fig. 6 between the double arrowheads and followed with a dotted line. This arrival dips steeply with a slope corresponding to a wave speed of 5220 m/s, which is representative of an extensional or bar wave propagating through the PQ steel casing (e.g., Drumheller 1989). The character of this event changes abruptly near 160 m depth, at which point an upward-going reflection is seen and the downward-going amplitude is substantially diminished. This is likely due to the

Table 1. A simplified processing flow chart for the application of the median filter method.

| Step | Process | Comments and rationale |
|---|---|---|
| 1 | Pick P-wave arrival times | |
| 2 | Apply bandpass filter | Remove air gun bubble reverberation (Fig. 8b) |
| 3 | Time shift traces such that the first arrivals are at the same time | This is an integral step to application of the median filter method. There are also advantages in applying the next step on flattened traces. |
| 3 | Apply f-k filter to remove down-going secondary wave | The down-going secondary wave amplitudes contaminate those of the down-going P-wave |
| 4 | Equalize amplitudes of flattened P-arrivals | Makes all of these as similar as possible, required for application of the median filter |
| 5 | Apply median filter | Provides estimate of down-going pulse at each depth |
| 6 | Subtract result of step 5 from result of step 4 | Difference is the up-going portion of the wave field |
| 7 | Time shift back this result | Returns to the original times |
| 8 | Display up-going wave field | See Fig. 8c |

Table 2. A simplified processing flow chart for the application of the f-k filter method.

| Step | Process | Comments and rationale |
|---|---|---|
| 1 | Pick P-wave arrival times | |
| 2 | Apply bandpass filter | Remove air gun bubble reverberation Fig. 8b |
| 3 | Time shift traces such that the first arrivals are at the same time | Advantages to employing f-k filter in flattened profile |
| 4 | Take 2-D FFT of flattened profile | |
| 5 | Remove low and negative wave number sections of 2-D FFT | Simplified way to remove all down-going arrivals. Remaining portions of 2-D spectrum are primarily up-going arrivals. |
| 6 | Take 2-D IFFT | Reforms the up-going arrivals in depth-time space |
| 7 | Time shift back this result | Returns to the original times |
| 8 | Display up-going wave field | See Fig. 8d |

coupling of the PQ steel casing to the lake sediments at depths below 160 m. This first arriving steel casing-related extensional wave arrival is problematic, as it obscures the more useful geological information.

A second weak arrival (delineated in Fig. 6 between the single large arrowhead at 50 m and by the point of the white arrowhead at 239 m depth) propagates downward at a speed close to 1520 m/s. This value is not that different from the speed of sound in water and consequently allows for two possible interpretations. First, it may be the true P-wave traveling first through the lake water and then the lake sediments. This velocity is in relatively good agreement with the Karp et al.(2002) seismic model shown in Fig. 3, and with the earlier constraints placed on sound velocities in soft marine sediments by Hamilton (1985) An alternative explanation is that the weak arrival is one type of “tube wave” that is a coupled and dispersive mode propagating along a fluid filled tube surrounded an elastic solid medium (Biot 1952). We prefer the former explanation because the strong and unambiguous direct P-wave arrival in the lower open-hole section of the borehole is continuous with this arrival.

**Open Hole Section**

Two coherent arrivals are seen in the lower open hole section of the borehole, as indicated in Fig. 6. Both originate at the same time and depth as the termination of the sediment arrival through the casing described above. The direct compressional wave arrival is indicated between the white arrow at 239 m and the black arrowhead at 450 m depth. A secondary arrival trends between the white arrowhead at 239 m depth and the triple arrow head near 390 m depth.

Sonic logging provided measures of the interval velocities with depth at frequencies of ~20 kHz (Fig. 9a). Direct comparison of sonic log velocities to those measured from the VSP data is difficult due to frequency dependent dispersion resulting from both scale and rock property dependent effects (e.g., Sams et al. 1997). Here, comparison is facilitated by smoothing the sonic curve using a variety of averages that include the simple arithmetic mean:

$$V_A(z) = \frac{\sum V_P(z_i)}{N} \quad (1)$$

a long-wavelength approximation $V_B$ based on a Backus average in a constant density medium (e.g., Rio et al. 1996):

$$V_B z = \left[\frac{\sum V_P^{-2}(z_i)}{N}\right]^{-1/2} \quad (2)$$

and a high-frequency, ray theory time or harmonic average $V_W$:

$$V_W(z) = \frac{N}{\sum V_P^{-1}(z_i)} \quad (3)$$

where $N$ is the number of contiguous sonic log samples $V_P(z_i)$ over the range of depths centered on $z$. $N$ is chosen sufficiently large to allow the smoothing averages to be calculated over a depth range comparable to the wavelength of the seismic data; 10 m was selected for the calculations shown. The arithmetic mean is not physically meaningful in the context of rates, but due to its simplicity in smoothing it is widely employed and

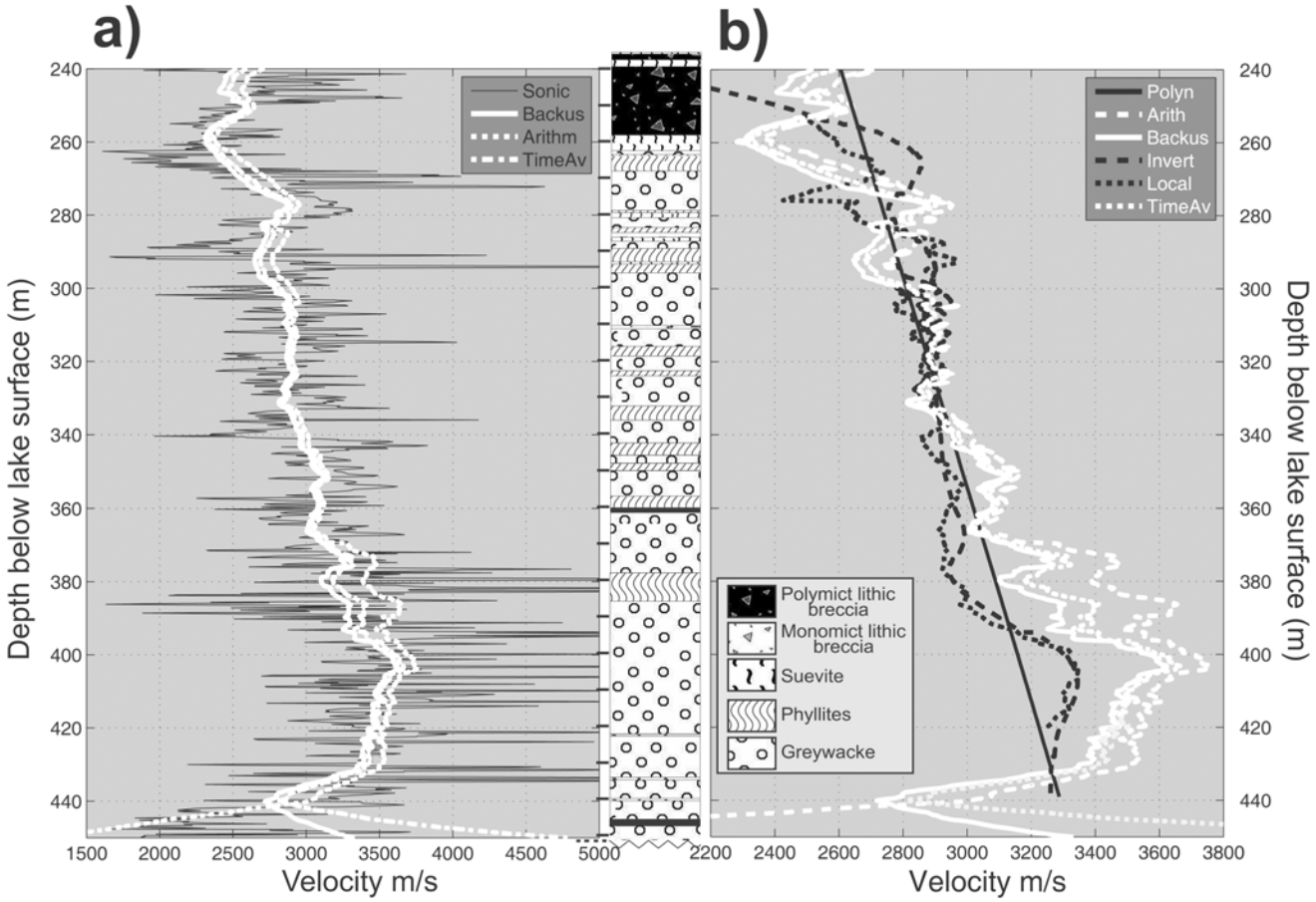


Fig. 9. Measures of interval velocities over open hole section. a) Observed sonic log interval velocities (thin line) with corresponding Backus average (solid white line), time average (dashed line), and arithmetic average (dotted white line). b) Sonic log averages from (a) (white lines) compared to values of the interval velocity obtained from the seismic travel times of Fig. 8 using a simple polynomial fit (solid black line), inversion (dashed black line), and local linear slope (dotted black line). Note expansion of velocity scale from (a) to (b). The central panel is the preliminary simplified geological core log for LB-08A as developed by A. Deutsch, L. Ferrière, C. Koeberl, and S. Luetke. The legend describing the lithologies is provided as an insert in the lower left of Fig. 9b.

has been included for purposes of comparison. Otherwise, $V_B$ and $V_W$ do have physical interpretations and represent the expected low and high frequency limits of the velocities of a stack of layers of velocity $V_P(z_i)$ and thickness $z$ (here equal to 10 cm). Ignoring edge effects in the calculations, $V_A > V_W > V_B$ in Fig. 9a. Regardless of the average employed, the trend of the smoothed sonic velocities generally increases with depth from ~2500 m/s to ~3400 m/s. There is no clear relationship between the velocity and the lithology (central panel of Fig. 9).

The seismic $V_p(z)$ of Fig. 9b were determined in the open hole zone from the picked travel times with depth using three methods: 1) by differentiation of the travel time curve obtained by least-squares quadratic-curve fitting $V_{FP}$, 2) by inversion of the picked times using a damped least squares minimization $V_{IP}$ (Lizarralde and Swift 1999), and 3) by estimation of the local tangent slope of the travel time curve by least squares fitting of a line to a number of contiguous time picks $V_{LP}$.

The least-squares quadratic-fitting of these travel times (Fig. 9b) provides the trend of velocity with depth and yields a model for the waves travel time $t$ (in ms) as a function of depth $z$ (in m) of:

$$t(z) = -2.03 \times 10^{-4} z^2 + 0.478z + 59.9 \quad (4)$$

with a correlation coefficient better than 0.998. The wave speed $V_p$ with depth is then estimated from the simple differentiation of Equation 3 to give:

$$V_{FP}(z) = \frac{1}{0.478 - 4.06 \times 10^{-4} z} \quad (5)$$

valid in the range of depths between 239 m and 439 m. This curve fitting indicates that the P-wave velocity in the hard rock increases from 2610 m/s at 239 m to 3340 m/s at 439 m. Both the inversion $V_{IP}$ and the local slope $V_{LP}$ seismic interval velocities agree well (Fig. 9b) and confirm the trend of increasing velocity with depth.

These seismic wave speeds are also compared to the P-wave sonic log in Fig. 9b. Briefly, the sonic log measures the P-wave velocity by obtaining the wave transit time over an interval of 1 m with a measurement made every 0.1 m along the well bore. Sonic log tools transmit waves with frequencies on the order of 20 kHz and decimeter scale wavelengths. They provide a complementary measure of in situ velocities to the seismic velocities, which here fall in the band from 15 Hz to 150 Hz with wavelengths greater than 10 m. As is apparent in Fig. 9b, the seismic wave field is insensitive to the small scale variations in the rock properties that are detected by the higher frequency logging of Fig. 9a. Aside from the zone between 300 m and 340 m depth, the variations between the seismic and the sonic log values can be considerable, reaching ~10% near 400 m depth. As noted above, such variations are generally observed. (Stewart et al. 1984) but with the seismic velocities lower than the sonic as, is the case below 340 m.

The preliminary lithological core log (central panel of Fig. 9) of Koeberl et al. (2007) suggests that the lithologies in LB-08A are primarily meta-graywacke irregularly intercalated with metapelite. This section is capped with a polymict impact breccia layer. A few thin suevite dikes intersect the core as well. It is not yet clear how the variations in the sonic log relate to the heterogeneous lithology and it is doubtful, given the weak degree of metamorphism experienced by these materials, that one can ascribe a distinct range of velocities to any of the rock types observed in the core. Despite this difficulty, however, the observed seismic and sonic velocities are substantially lower than expected for their rock type. For comparison, pore-free monocrystalline, isotropic aggregates of quartz and muscovite, representative of the main minerals in the rocks, have velocities of 6050 m/s (Bass 1995) and 5700 m/s (Cholach and Schmitt 2006), respectively.

The velocity of the second weak arrival, observed in Fig. 6 and heretofore referred to as the secondary wave, is estimated using least squares polynomial-fitting of the travel times shown in Fig. 7. Its moveout $t_s$ is best described by the quadratic:

$$t_s(z) = -4.13 \times 10^{-4} z^2 + 1.20z - 92.7 \quad (6)$$

with a correlation coefficient better than 0.98. The velocity $V_{FS}(z)$ given by the derivative of Equation 6 is:

$$V_{FS}(z) = \frac{1}{1.20 - 8.26 \times 10^{-4} z} \quad (7)$$

valid between 239 m and 390 m depth. $V_{FS}$ increases monotonically from 1000 m/s to 1110 m/s over this depth range (this trend is compared to the $V_{FP}(z)$ in Fig. 10).

Although it is tempting to interpret this secondary wave as a shear wave, its velocity is low relative to expectations. The $V_p/V_s$ ratio is often a useful comparative measure and for many metamorphic rocks will have a value near 1.7 (e.g., Ji et al. 2002). Here, the ratio of the P-wave velocity to that of the secondary wave increases with depth from 2.5 to 2.7. On the other hand, it is difficult to attribute the observed arrivals to a tube wave, which as noted above typically travels at near the velocity of the borehole fluid (~1500 m/s for water). With the current observations, it may not be possible to unambiguously determine what type of wave mode is seen.

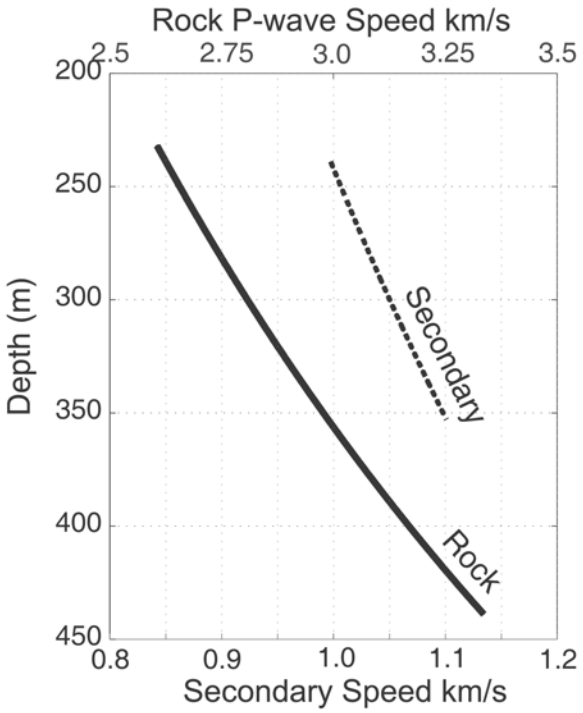


Fig. 10. A comparison of compressional P-wave and secondary wave velocities as determined using polynomial fitting.

As noted, it has long been known that the compressibility of "crystalline" hard rocks increases nonlinearly with confining stress due to the progressive closure of small crack-like porosity. These microcracks are highly compliant at low confining stresses. Application of increasing confining stress will close such cracks at a pressure that depends on factors such as the crack length and the rock's mineral elastic properties. A closed crack no longer influences the overall elasticity of the rock. Most rocks will contain families of microcrack porosity with a variety of lengths and apertures. Consequently, as confining pressure increases the cracks progressively close; the material becomes stiffer and the P- and S-wave velocities both increase. The increase in the velocity with pressure eventually flattens once most of the cracks are closed, whereupon the velocity is then representative of that expected for the pore-free mineral assemblage. We refer to this state of stress as the crack closure pressure $P_c$.

Although no hard and fast rules exist with respect to the variability of the porosity found in such rocks, some more general observations from the literature can be made with

regards to the influence of such porosity on the seismic wave speeds. The literature on the determination of velocity in such rocks is large but some contributions that illustrate the points below include Adams and Williamson (1923), Birch (1960), Christensen (1965, 1966), and Salisbury and Fountain (1994). First, the increase in the wave speed of such rocks over the range from room pressure to $P_c$ is typically less than 20%. Some extreme cases of highly damaged core retrieved from depths of nearly 12 km in the Kola Peninsula (Russia), scientific borehole displayed changes of nearly 30%, but such variations are unusual (Vernik et al. 1994; Kern et al. 2001).

There are two main points to summarize: i) the velocities observed are substantially lower than is expected for such rock types, and ii) the velocities increase by 30% over a very small increase of confining pressure. A possible interpretation of this result is that the rock retains extensive microcrack damage and, further, that the degree of this damage decreases with depth. These results appear to be in qualitative agreement with the recent thermal conductivity measurements of Popov et al. (2003) on archived core obtained from the Nördlingen 1973 research borehole drilled in the Ries impact structure. Thermal conductivity was found to generally increase with depth, as did the P-wave sonic log velocities. Inverse modeling of these results showed that porosity tended to decrease with depth, while the pore shapes evolved from crack-like to more equant.

## CONCLUSIONS

Borehole seismic measurements were carried out in the hard rock Bosumtwi borehole LB-08A. The seismic wave field was densely sampled with a recording point at every meter along the borehole. Although the final compiled set of seismic traces shows a complex pattern in the upper cased section of the well, a strong and distinct direct P-wave first arrival is seen in the hard-rock open hole section from 239 m to 451 m in depth.

The P-wave velocity was determined from travel time picking of this phase and suggested that the seismic velocity increased by nearly 30% over the 211 m of the open hole interval from 2600 m/s to 3340 m/s. This trend is also apparent in the corresponding sonic velocities. A weak secondary arrival, possibly the shear wave, was also detected in the open hole section. The velocities of this mode varied from 1000 m/s to 1110 m/s. Otherwise, the observed velocities agree well with those estimated in earlier surface based refraction and reflection studies at Lake Bosumtwi and are consistent with observations beneath similar impact craters.

It is not yet known to what degree the velocity depends on the geologically interpreted rock types. In any event, the observed velocities are substantially below those generally anticipated for metasedimentary rocks. One possible interpretation of this is that the rocks are highly damaged due to the direct shock and the release wave deformations during the impact event. The rapid increase in the velocity trend with depth may be indicative of the level of shock deformation with distance from the impact point. Conversely, the variation in velocity with depth may provide a proxy for the degree of shock damage, which in turn could provide some measure of the shock pressures and other deformational strain experienced by the rock during the formation of the crater. However, this relatively large increase in seismic velocity is observed over a 220 m range of depths, which is small relative to the zones of damage predicted to extend to at least 5 km below the crater floor by the numerical modeling of Artemieva et al (2004).

Resolution of this issue mandates further detailed studies of the pore structures within the core. Some initial work has already suggested there is no correlation between porosity and depth (Brown et al. 2006). This work is currently followed up by more extensive Hg injection porosimetry in conjunction with scanning electron and thin section microscopy to examine the details of the pore space.

*Acknowledgments*–The measurements were greatly assisted by L. Tober and J. Lapukini, and the GFZ logging team of J. Kuck, C. Carnein, and M. Toepfer. Drilling at Bosumtwi was supported by the International Continental Drilling Program (ICDP), the U.S. NSF-Earth System History Program under Grant No. ATM-0402010, Austrian FWF (project P17194-N10), the Austrian Academy of Sciences, and by the Canadian NSERC. Drilling operations were performed by DOSECC. Local help by the Geological Survey Department (Accra) and KNUST (Kumasi), Ghana, was invaluable.

*Editorial Handling*—Dr. Wolf Uwe Reimold

## REFERENCES

Ackermann H. D., Godson R. H., and Watkins J. S. 1975. Seismic refraction technique used for subsurface investigations at Meteor Crater, Arizona. *Journal of Geophysical Research* 80:765–775.

Ackermann H. D., Grow J. A., and Williams J. M. 1986. Seismic refraction survey of OAK crater. *United States Geological Survey Bulletin* 1678:E1–E18.

Adams L. H. and Williamson E. D. 1923. On the compressibility of minerals and rocks at high pressures. *Journal of the Franklin Institute* 195:475–529.

Ahrens T. J. and Rubin A. M. 1993. Impact-induced tensional failure in rock. *Journal of Geophysical Research* 98:1185–1203.

Ai H. A. and Ahrens T. J. 2004. Dynamic tensile strength of terrestrial rocks and application to impact cratering. *Meteoritics & Planetary Science* 39:233–246.

Ai H. A. and Ahrens T. J. 2007. Effects of shock-induced cracks on the ultrasonic velocity and attenuation in granite. Journal of *Geophysical Research* 112:B01201, doi:10.1029/2006JB004353.

Amundsen L., Ikelle L. T., and Berg L. E. 2001. Multidimensional signature deconvolution and free-surface multiple elimination of

marine multicomponent ocean-bottom seismic. *Geophysics* 66: 1594–1604.

Artemieva N., Karp T., and Milkereit B. 2004. Investigating the Lake Bosumtwi impact structure: Insight from numerical modeling. *Geochemistry Geophysics Geosystems* 5: Q11016, doi:10.1029/2004GC000733.

Åström K. 1998. Seismic signature of the lake Mien impact structure, southern Sweden. *Geophysical Journal International* 135:215–231.

Bass J. D. 1995. Elasticity of minerals, glasses, and melts. In *Mineral physics and crystallography: A handbook of physical constants*, edited by Ahrens T. J. Washington, D.C.: American Geophysical Union. pp. 45–63.

Beydoun W. B., Cheng C. H., and Toksöz M. N. 1985. Detection of open fractures with vertical seismic profiling. *Journal of Geophysical Research* 90:4557–4566.

Biot M. A. 1952. Propagation of elastic waves in a cylindrical bore containing a fluid. *Journal of Applied Physics* 23:997–1005.

Birch F. 1960. The velocity of compressional waves in rocks to 10-kilobars. *Journal of Geophysical Research* 65:1083–1102.

Boerner D. E., Milkereit B., and Davidson A. 2000. Geoscience impact: A synthesis of studies of the Sudbury structure. *Canadian Journal of Earth Sciences* 37:477–501.

Brown M., Schmitt D. R., Milkereit B., and P. Claeys. 2006. Porosity in impact-damaged rocks: Inferences from scientific drilling in the Lake Bosumtwi, Ghana, impact structure (abstract #1507). 37th Lunar and Planetary Science Conference. CD-ROM.

Cholach P. Y. and Schmitt D. R. 2006. Intrinsic elasticity of a textured phyllosilicate aggregate: Relation to the seismic anisotropy of shales and schists. *Journal of Geophysical Research* 111: B09410, doi:10.1029/2005JB004158.

Christensen M. I. and Mooney W. D. 1995. Seismic velocity structure and composition of the continental crust—A global view. *Journal of Geophysical Research* 100:9761–9788.

Christensen N. I. 1965. Compressional wave velocities in metamorphic rocks at pressures to 10 kilobars. *Journal of Geophysical Research* 70:6147–6164.

Christensen N. I. 1966. Shear wave velocities in metamorphic rocks at pressures to 10 kilobars. *Journal of Geophysical Research* 71: 5921–5931.

Cicerone R. D. and Toksöz M. N. 1995. Fracture characterization from vertical seismic profiling data. *Journal of Geophysical Research* 100:4131–4148.

Collins G. S., Melosh H. J., and Ivanov B. A. 2004. Modeling damage and deformation in impact simulations. *Meteoritics & Planetary Science* 39:217–231.

Coney L., Gibson R., Reimold W. U., and Koeberl C. 2007. Lithostratigraphic and petrographic analysis of the ICDP drill core LB-07A from the Bosumtwi impact structure, Ghana. *Meteoritics & Planetary Science* 42. This volume.

Deutsch A., Luetke S., and Heinrich V. 2007. Lake Bosumtwi impact crater scientific drilling project (Ghana): Core LB-08A litho-log. *Meteoritics & Planetary Science* 42. This volume.

Drumheller D. S. 1989. Acoustical properties of drill strings. *Journal of the Acoustical Society of America* 85:1048–1064.

Durrheim R. J. and Green R. W. E. 1992. A seismic refraction investigation of the archean Kaapvaal craton, South Africa, using mine tremors as the energy source. *Geophysical Journal International* 108:812–832.

Dypvik H., Mork A., Smelror M., Sandbakken P. T., Tsikalas F., Vigran J. O., Bremer G. M. A., Nagy J., Gabrielsen R. H., Faleide J. I., Bahiru G. M., and Weiss H. M. 2004. Impact breccia and ejecta from the Mjølnir crater in the Barents sea—The Ragnarok formation and Sindre bed. *Norwegian Journal of Geology* 84: 143–167.

Ferrière L., Koeberl C., and Reimold W. U. 2007. Bosumtwi impact structure Ghana: Petrographic and shock metamorphic studies of rocks from the central uplift. *Meteoritics & Planetary Science* 42. This volume.

Florensky P. and Dabizha A. 1980. *Zhamanshin meteorite crater*. Moscow: Nauka. 128 p.

Gebhardt A. C., Niessen F., and Kopsch C. 2006. Central ring structure identified in one of the world's best-preserved impact craters. *Geology* 34:145–148.

Gibson R. L. and Reimold W. U. 2001. *The Vredefort impact structure, South Africa (The scientific evidence and a two-day excursion guide)*. Memoir #92. Pretoria: Council for Geoscience. 110 p.

Gibson R. and Reimold W. U. 2005. *Meteorite impact! The danger from space and South Africa's mega-impact, the Vredefort impact*. Johannesburg: Chris van Rensburg Publications. 319 p.

Green R. W. and Chetty P. 1990. Seismic refraction studies in the basement of the Vredefort structure. *Tectonophysics* 171:105–113.

Hajnal Z., Scott D., and Robertson P. B. 1988. Reflection study of the Haughton impact crater. *Journal of Geophysical Research* 93: 11,930–11,942.

Hamilton E. L. 1985. Sound-velocity as a function of depth in marine-sediments. *Journal of the Acoustical Society of America* 78:1348–1355.

Hardage B. 2000. *Vertical seismic profiling: Principles*, 3rd ed. Amsterdam: Pergamon Press. 552 p.

Hargreaves N. D. 1992. Air-gun signatures and the minimum-phase assumption. *Geophysics* 57:263–271.

Harris J. B., Jones D. R., and Street R. L. 1991. A shallow seismic refraction study of the Versailles cryptoexplosion structure, central Kentucky. *Meteoritics* 26:47–53.

He H. L. and Ahrens T. J. 1994. Mechanical properties of shock-damaged rocks. *International Journal of Rock Mechanics and Mining Sciences and Geomechanics Abstracts* 31:525–533.

Hinds R., Anderson N., and Kuzimski R. 1996. *VSP interpretive processing: Theory and practice*. Tulsa, Oklahoma: Society of Exploration Geophysicists. 205 p.

Ji S., Wang Q., and Xia B. 2002. *Handbook of seismic properties of minerals, rocks, and ores*. Montreal: Polytechnic International Press. 630 p.

Johnson D. T. 1994. Understanding air-gun bubble behavior. *Geophysics* 59:1729–1734.

Jones W. B., Bacon M., and Hastings D. A. 1981. The Lake Bosumtwi impact crater, Ghana. *Geological Society of America Bulletin* 92:1342–1349.

Karp T., Milkereit B., Janle P., Danuor S. K., Pohl J., Berckhemer H., and Scholz C. A. 2002. Seismic investigation of the Lake Bosumtwi impact crater: Preliminary results. *Planetary and Space Science* 50:735–743.

Kern H., Popp T., Gorbatsevich F., Zharikov A., Lobanov K. V., and Smirnov Y. P. 2001. Pressure and temperature dependence of VP and VS in rocks from the superdeep well and from surface analogues at Kola and the nature of velocity anisotropy. *Tectonophysics* 338:113–134.

Knight R. and Nolen-Hoeksema R. 1990. A laboratory study of the dependence of elastic wave velocities on pore scale fluid distribution. *Geophysical Research Letters* 17:1529–1532.

Koeberl C., Bottomley R., Glass B. P., and Storzer D. 1997. Geochemistry and age of Ivory Coast tektites and microtektites. *Geochimica et Cosmochimica Acta* 61:1745–1772.

Koeberl C. and Reimold W. U. 2005. Bosumtwi impact crater, Ghana (West Africa): An updated and revised geological map with explanations. *Jahrbuch der Geologischen Bundesanstalt, Wien*

(*Yearbook of the Austrian Geological Survey*) 145:31–70 (+1 map, 1:50,000).

Koeberl C., Milkereit B., Overpeck J. T., Scholz C. A., Amoako P. Y. O., Boamah D., Danuor S. K., Karp T., Kueck J., Hecky R. E., King J. W., and Peck J. A. 2007. An international and multidisciplinary drilling project into a young complex impact structure: The 2004 ICDP Bosumtwi impact crater, Ghana, drilling project—An overview. *Meteoritics & Planetary Science* 42. This volume.

Kommendal J. and Tjostheim B. 1989. A study of different methods of wavefield separation for application to VSP data. *Geophysical Prospecting* 37:117–142

L'Heureux E. and Milkereit B. 2007. Impactites as a random medium—Using variations in physical properties to assess heterogeneity within the Bosumtwi meteorite impact crater. *Meteoritics & Planetary Science* 42. This volume.

Lay T. and Wallace T. C. 1995. *Modern global seismology.* San Diego: Academic Press. 517 p.

Li Y. D., Rabbel W., and Wang R. 1994. Investigation of permeable fracture-zones by tube-wave analysis. *Geophysical Journal International* 116:739–753.

Liu C. L. and Ahrens T. J. 1997. Stress wave attenuation in shock-damaged rock. *Journal of Geophysical Research* 102:5243–5250.

Lizarralde D. and Swift S. 1999. Smooth inversion of VSP traveltime data. *Geophysics* 64:659–661.

Molyneux J. B. and Schmitt D. R. 2000. Compressional-wave velocities in attenuating media: A laboratory physical model study. *Geophysics* 65:1162–1167.

Moon W., Carswell A., Tang R., and Dilliston C. 1986. Radon-transform wave field separation for vertical seismic profiling data. *Geophysics* 51:940–947.

Morgan J. V., Warner M. R., Collins G. S., Melosh H. J., and Christenson G. L. 2000. Peak-ring formation in large impact craters: Geophysical constraints from Chicxulub. *Earth and Planetary Science Letters* 183:347–354.

O'Connell R. J. and Budiansky B. 1974. Seismic velocities in dry and saturated cracked solids. *Journal of Geophysical Research* 79: 5412–5426.

Papasikas N. and Juhlin C. 1997. Interpretation of reflections from the central part of the Siljan ring impact structure based on results from the Stenberg-1 borehole. *Tectonophysics* 269:237–245.

Phillips F. M., Zreda M. G., Smith S. S., Elmore D., Kubik P. W., Dorn R. I., and Roddy D. J. 1991. Age and geomorphic history of Meteor crater, Arizona, from cosmogenic $Cl^{36}$ and $C^{14}$ in rock varnish. *Geochimica et Cosmochimica Acta* 55:2695–2698.

Pilkington M. and Grieve R. A. F. 1992. The geophysical signature of terrestrial impact craters. *Reviews of Geophysics* 30:161–181.

Pohl J. and Will M. 1974 Vergleich der geschwindigkeitsmessungen im bohrolch der forschungsbohrung Nördlingen 1973 mit seismischen tiefensondierungen innerhalb und ausserhalb des Ries. *Geologica Bavarica* 72:75–80.

Pohl J., Stöffler D., Gall H., and Ernstson K. 1977. The Ries impact crater. In *Impact and explosion cratering*, edited by Roddy D. J., Pepin R. O., and Merril R. B. New York: Pergamon Press. pp. 343–404.

Polanskey C. A. and Ahrens T. J. 1990. Impact spallation experiments—Fracture patterns and spall velocities. *Icarus* 87: 140–155.

Popov Y., Pohl J., Romushkevich R., Tertychnyi V., and Soffel H. 2003. Geothermal characteristics of the Ries impact structure. *Geophysical Journal International* 154:355–378.

Reimold W. U., Brandt D., and Koeberl C. 1998. Detailed structural analysis of the rim of a large, complex impact crater: Bosumtwi crater, Ghana. *Geology* 26:543–546.

Rio P., Mukerji T., Mavko G., and Marion D. 1996. Velocity dispersion and upscaling in a laboratory-simulated VSP. *Geophysics* 61:584–593.

Salisbury M. H. and Fountain D. M. 1994. The seismic velocity and Poisson's ratio structure of the Kapuskasing uplift from laboratory measurements. *Canadian Journal of Earth Sciences* 31:1052–1063.

Sams M. S., Neep J. P., Worthington M. H., and King M. S. 1997. The measurement of velocity dispersion and frequency-dependent intrinsic attenuation in sedimentary rocks. *Geophysics* 62:1456–1464.

Scholz C. A., Karp T., Brooks K. M., Milkereit B., Amoako P. Y. O., and Arko J. A. 2002. Pronounced central uplift identified in the Bosumtwi impact structure, Ghana, using multichannel seismic reflection data. *Geology* 30:939–942.

Scholz C. A., Karp T., and Lyons R. P. 2007. Structure and morphology of the Bosumtwi impact structure from seismic reflection data. *Meteoritics & Planetary Science* 42. This volume.

Scott D. and Hajnal Z. 1988. Seismic signature of the Haughton structure. *Meteoritics* 23:239–247.

Seeman B. and Horowicz L. 1983. Vertical seismic profiling—Separation of upgoing and downgoing acoustic waves in a stratified medium. *Geophysics* 48:555–568.

Stewart R. R., Huddleston P. D., and Kan T. K. 1984. Seismic versus sonic velocities—A vertical seismic profiling study. *Geophysics* 49:1153–1168.

Stewart S. A. and Allen P. J. 2005. 3D seismic reflection mapping of the Silverpit multi-ringed crater, North Sea. *Geological Society of America Bulletin* 117:354–368.

Therriault A. M., Fowler A. D., and Grieve R. A. F. 2002. The Sudbury igneous complex: A differentiated impact melt sheet. *Economic Geology and the Bulletin of the Society of Economic Geologists* 97:1521–1540.

Vernik L., Hickman S., Lockner D., and Rusanov M. 1994. Ultrasonic velocities in cores from the Kola superdeep well and the nature of subhorizontal seismic reflections. *Journal of Geophysical Research* 99:24,209–24,219.

Wu J. J., Milkereit B., and Boerner D. E. 1995. Seismic imaging of the enigmatic Sudbury structure. *Journal of Geophysical Research* 100:4117–4130.

Wünnemann K., Morgan J. V., and Jodicke H. 2005. Is Ries crater typical for its size? An analysis based upon old and new geophysical data and numerical modeling. In *Large meteorite impacts III*, edited by Kenkmann T., Hörz F., and Deutsch A. Boulder, Colorado: Geological Society of America. pp. 67–83.

Xia K. W. and Ahrens T. J. 2001. Impact-induced damage beneath craters. *Geophysical Research Letters* 28:3525–3527.

Yilmaz Ö. 2001. *Seismic data analysis: Processing, inversion, and interpretation of seismic data*, 2nd ed. Tulsa, Oklahoma: Society of Exploration Geophysicists. 526 p.

Ziolkowski A. 1991. Why don't we measure seismic signatures? *Geophysics* 56:190–201.